Neutron emission generated during wire array Z-pinch implosion onto deuterated fiber

D. Klir,[1] J. Kravarik,[1] P. Kubes,[1] K. Rezac,[1] S. S. Anan'ev,[2] Yu. L. Bakshaev,[2] P. I. Blinov,[2] A. S. Chernenko,[2] E. D. Kazakov,[2] V. D. Korolev,[2] B. R. Meshcherov,[2] G. I. Ustroev,[2] L. Juha,[3] J. Krasa,[3] and A. Velyhan[3]
[1]*Czech Technical University, Faculty of Electrical Engineering, Department of Physics, Technicka 2, 166 27 Prague 6, Czech Republic*
[2]*Russian Research Center, Kurchatov Institute, 1 Kurchatov Sq., 123182 Moscow, Russia*
[3]*Institute of Physics, Na Slovance 2, 182 21 Prague 8, Czech Republic*

(Received 20 November 2007; accepted 10 January 2008; published online 12 March 2008)

The implosion of both cylindrical and conical wire arrays onto a deuterated polyethylene fiber was studied on the S-300 pulsed power generator [A. S. Chernenko *et al.*, *Proceedings of the 11th International Conference on High Power Particle Beams* (Academy of Science of Czech Republic, Prague, 1996), p. 154]. Neutron measurements were used to obtain information about acceleration of fast deuterons. An average neutron yield approached 10^9 on the current level of 2 MA. In the case of conical wire arrays, side-on neutron energy spectra peaked at 2.48 ± 0.05 MeV with 450 ± 100 keV full width at half-maximum. In the downstream direction, the peak neutron energy and the width of a neutron spectrum were 2.65 ± 0.10 MeV and 350 ± 100 keV, respectively. The total number of fast deuterons was 10^{15} and their average kinetic energy was about 150 keV. Most of the deuterons were directed toward the cathode. The broad width of neutron spectra in the side-on direction implied a high radial component of deuteron velocity. With regard to the emission time, neutron pulses temporally correlated with hard x rays and also with measured voltage. The neutron emission lasted on average 30 ± 5 ns and it was observed during the stagnation and at the beginning of the expansion of a plasma column. At this moment, the plasma impedance reached 0.2–0.4 Ω. In the post-stagnation phase, this value was formed significantly by enhanced plasma resistance. Similar experimental results were observed also with cylindrical wire arrays imploding onto a deuterated fiber. © *2008 American Institute of Physics*. [DOI: 10.1063/1.2839352]

I. INTRODUCTION

At present, Z pinches belong to the most intensive laboratory sources of soft x rays,[1] and that is also the main reason why they are studied. The application of Z pinches as neutron sources has been somewhat problematic from the beginning of Z-pinch research primarily because of serious doubts in issues of crucial importance. More specifically, two fundamental questions have been studied: (i) the origin of neutrons and (ii) the scaling of a neutron yield with a current. In order to solve these questions and to achieve a higher neutron yield, various types of Z-pinch configurations have been tested from that time on.

In the 1950s, the controlled thermonuclear research was conducted with toroidal and straight compressional Z pinches mainly in the United Kingdom,[2] the United States,[3,4] the former Soviet Union,[5] but also in Canada, Germany, Japan, and Sweden.[6] During that time, teams of researchers were concerned with the idea of heating and confining a fusion mixture within a small diameter by a pinch effect. In compressional Z pinches, an electric current started at an insulating wall, and when a magnetic pressure exceeded a gas pressure, a current-carrying plasma shell together with a preceding shock wave radially collapsed. In the late 1950s, the researchers arrived at the conclusion that neutrons in Z pinches were not produced by thermal collisions of deuterons. This conclusion led to the abandonment of the straight Z pinch as a fusion power source. As a result, more complex schemes of magnetically confined plasma devices (such as θ pinches, stellarators, and tokamaks) were suggested and researched.

During the research of one of more stable schemes, namely Scylla θ pinch at Los Alamos, a plasma gun was used to inject a plasma into the device.[7] In this configuration, the plasma was accelerated between two coaxial electrodes. During the investigation of how the plasma gun worked, it was found that a large number of neutrons (up to 2×10^{10}) was generated from this plasma gun itself. This was the main reason why the so-called Mather-type plasma focus was researched from that time on. The maximum yield exceeded the value of 10^{12} neutrons per pulse.[8] In the former Soviet Union, the Filippov-type plasma focus was constructed independently from a gas embedded Z pinch with a conducting wall.[5,9]

The progress in nanosecond pulsed-power technology in the 1970s led to new attempts to use Z pinches in fusion research. A new effort was made at Los Alamos during high density Z-pinch experiments. It was known that a 100 μm current channel had to be created in order to reach fusion conditions (10^{26} m^{-3} density, 1 μs confinement time, 10 keV temperature) with the Pease–Braginski current of 1.4 MA.[10] It thus seemed reasonable enough to start with a small initial diameter of a plasma column. The idea was to initiate the

pinch by a focused laser or electron beam that would ionize a channel on the axis of a gas filled vessel. This is how a gas-embedded pinch is formed. Gas-embedded experiments demonstrated the possibility of producing stable Z pinches. However, the pinched plasma could not reach a high enough temperature because it rapidly accreted particles from the surrounding gas.

One suggestion on how to overcome the accretion and how to confine a high-density and high-temperature plasma column within a small diameter was to initiate Z pinches from fibers of cryogenic solid deuterium in vacuum.[11] Z-pinch plasmas in the first fiber experiments seemed to be stable for many radial Alfven transit times, whereas the neutron yield approached 10^{10} (Ref. 12). However, the enhanced stability was not confirmed in further and better diagnosed experiments on new generators at NRL[13] and Los Alamos[14] as well as on KALIF at Kernforschungszentrum Karlsruhe[15] or on MAGPIE at Imperial College in London.[16] Particularly, the early development of plasma instabilities and the rapid expansion decreased a plasma density substantially and thus eliminated the possibility of using a fiber Z pinch as a fusion reactor.

During fiber Z-pinch experiments, fibers from deuterated polyethylene were also employed because they were easily available in comparison with frozen deuterium fibers and at the same time neutron yields were almost identical.[17] In the case of fiber pinches, neutrons originated from several points distributed over the entire length of a fiber. For some applications it seemed better to have more localized neutron emission. For that purpose, an X pinch (that is, two crossed fibers) was tried.[18] Another possibility of energy concentration into one localized region was to employ a vacuum spark[19] or to preform an $m=0$ instability in a Z-pinch load.[20,21]

In the 1990s, most Z-pinch experiments were carried out with imploding wire arrays or gas-puffs. So far, the highest neutron yields in Z pinches have been reached with gas-puffs. One of the first deuterium gas-puff experiments was carried on the Angara 5-1 device at Troitsk.[22] The characteristic feature of this experiment was the relatively small mass of a liner and the axial gradient of a linear density. This way, a very high neutron yield above 10^{12} neutrons per shot was reached at the current of "only" 2–3 MA. The strong anisotropy of neutron fluxes and neutron energy spectra gave evidence of deuterons accelerated to 200–500 keV energies. Even more DD fusion neutrons were generated on the Z machine with a double-shell deuterium gas-puff on the current level of 17 MA.[23] With regard to the overall neutron yield in this experiment, there is a hope of a large thermonuclear component because it is difficult to explain the yield of about 6×10^{13} neutrons by the beam-target mechanism.

On the basis of experimental results of several research groups (see Refs. 24 and 25), solid fibers appear less suitable than deuterium gas-puffs when a high neutron yield is required. Nevertheless, it seemed interesting to see what would happen if a deuterated fiber were put in the center of a wire array or a hollow gas-puff. Two shots (Nos. 293 and 294) with 240 aluminum wires imploding onto a $(CD_2)_n$ fiber were carried out on Sandia's Z machine in 1998 but the obtained results have not been published. On the Saturn generator, $(2.8\pm0.2)\times10^{12}$ neutrons were generated during the implosion of a hollow deuterium gas-puff onto a 250 μm deuterated polyethylene fiber located on the pinch axis.[24] In addition to such a high neutron yield, the neutron emission was almost isotropic.

This short overview brings us to the purpose of this paper, which is concerned with Z-pinch experiments in which a wire array imploded onto a deuterated fiber. Since results with aluminum wire arrays have already been published,[26] we focus in particular on experiments with conical tungsten wire arrays here. The purpose of our experiment is described in Sec. II. Section III provides the description of a current generator and diagnostics used in our experiment. Section IV brings forward the most important results we have obtained. Section V contains the overall discussion within the framework of other experiments.

II. PURPOSE OF OUR EXPERIMENT AND METHOD USED

The primary objective of our experiments at the S-300 generator is to get deeper insight into the process of generating fast electrons, ions, and hard x rays in Z-pinch plasmas. Whereas a large number of papers are devoted to studies of EUV, soft-, and hard-x-ray radiation, and in some cases electrons, information about fast ions is rather rare. At this point we can mention the recent measurement of an ion temperature in wire arrays. The Doppler width of iron spectral lines indicated that the ion temperature exceeded 200 keV.[27] Such a result suggests that also a fusion neutron measurement could provide invaluable data for Z-pinch physics since it helps us to understand the issue of the acceleration of fast ions. And that is precisely why we are interested in the research of fusion reactions in Z pinches.

At the S-300 generator, the easiest way to produce fusion neutrons seemed to be putting a deuterated fiber in the center of a wire array. As regards the fusion of two deuterons, there are two branches of the reaction. They both occur with nearly equal probability.

$$\mathrm{D}+\mathrm{D}\rightarrow \mathrm{T}\ (1.01\ \mathrm{MeV})+\mathrm{p}\ (3.02\ \mathrm{MeV}),$$

$$\mathrm{D}+\mathrm{D}\rightarrow {}^{3}_{2}\mathrm{He}(0.82\ \mathrm{MeV})+\mathrm{n}(2.45\ \mathrm{MeV}).$$

Since neutrons are influenced neither by magnetic nor by electric fields, the detection of neutrons is a favorable diagnostic tool for fast deuterons in a plasma. This very fact is also taken into account when studying plasmas not only in Z pinches but also in tokamaks,[28] nanosecond, and femtosecond lasers.[29] A great advantage of neutron diagnostics is weak absorption and scattering of neutrons in the air, which enables us to use the extended time-of-flight (TOF) analysis for the determination of neutron energy spectra.

The time-resolved neutron energy distribution function $f(E_n,t)$ can be reconstructed from time-resolved neutron signals $S(x,T)$, which are recorded by several detectors in one direction at different distances x. The relation between the neutron flux $S(x,T)$ and the energy distribution function $f(E_n,t)$ is given by

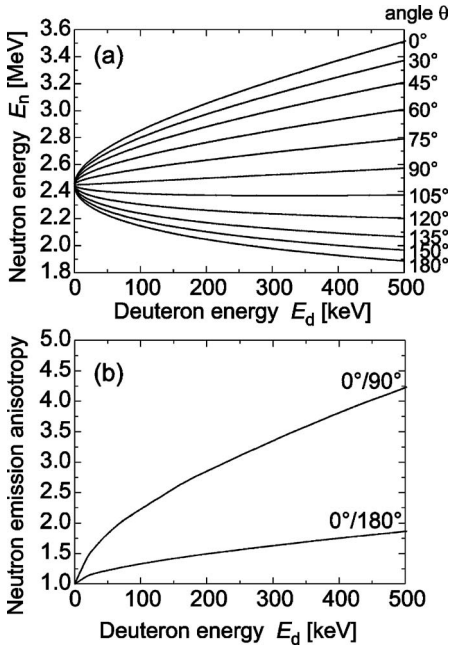

FIG. 1. (a) The energy-angle dependence of neutron energies for the $D(d,n)^3He$ fusion reaction. (b) The ratio between differential cross sections for θ=0°, 90°, and 180° as a function of a deuteron energy for the $D(d,n)^3He$ reaction. The angle θ is the laboratory angle between the incoming fast deuteron and the outgoing neutron.

$$S(x,T) = \int dt \int dE_n f(E_n,t)\,\delta\left(t - T + \frac{x}{\sqrt{2E_n/m_n}}\right), \qquad (1)$$

where E_n is the neutron energy, m_n is the neutron mass, T is the neutron detection time, and t is the emission time. It follows from this equation that the time of neutron production is estimated mainly from the nearest neutron signal and the energy of neutrons is determined mainly from the most distant neutron detector. There are several developed algorithms for the deconvolution of the $f(E_n,t)$ function. In our case, a Monte Carlo method[30] was used and subsequently improved. Our improvement is based on the fact that it is possible to use neutron detectors in mutually opposite directions. In other words, neutron spectra could be evaluated from the chain of neutron detectors on both sides of the neutron source. On the one hand, such a procedure significantly improved results of neutron spectra reconstruction[31] and limited the influence of scattered neutrons (see the Appendix). But on the other hand, neutron emission anisotropy had to be included into the Monte Carlo reconstruction. We included the anisotropy of neutron energies [see Fig. 1(a)] and differential cross sections [see Fig. 1(b)] into our reconstruction.[32] Recently, we have taken into account the fact that deuteron velocities could have an arbitrary direction with respect to the chain of neutron detectors (i.e., with respect to the line of sight). Our calculation of the anisotropy was based on the scattering theory. The nuclear data of the D–D fusion reaction were taken from Refs. 28, 33, and 34.

III. APPARATUS AND DIAGNOSTICS

A. Current generator and Z-pinch load

The implosion of a conical tungsten wire array Z pinch onto a deuterated fiber was studied on the S-300 device (4 MA peak current, 700 kV voltage, 100 ns rise time, 0.15 Ω impedance) at the Kurchatov Institute in Moscow.[35] In this paper, we present results from the experimental series of 15 shots at the current level of 2 MA. The diameter of a conical wire array was 10 and 7 mm at the anode and at the cathode, respectively. The wires were inclined at an angle of 13° to the array axis. The conical wire arrays consisted of 30 tungsten wires 7 μm in diameter. The deuterated polyethylene $(CD_2)_n$ fibers with diameters between 80 and 120 μm were placed on the axis of the array. The enrichment of deuterium in the polyethylene was higher than 98%. The mass percentage of tungsten, carbon, and deuterium ions in Z-pinch load was about 73%, 20%, and 7%, respectively.

B. Diagnostics

In order to study dynamics of Z-pinch plasmas, we applied optical, x-ray, and neutron diagnostics, part of which was described in Refs. 36 and 37. Each shot was observed with the following set of diagnostic tools (cf. Fig. 2):

(i) An optical streak camera was performed in the radial mode, i.e., with a slit perpendicular to the Z-pinch

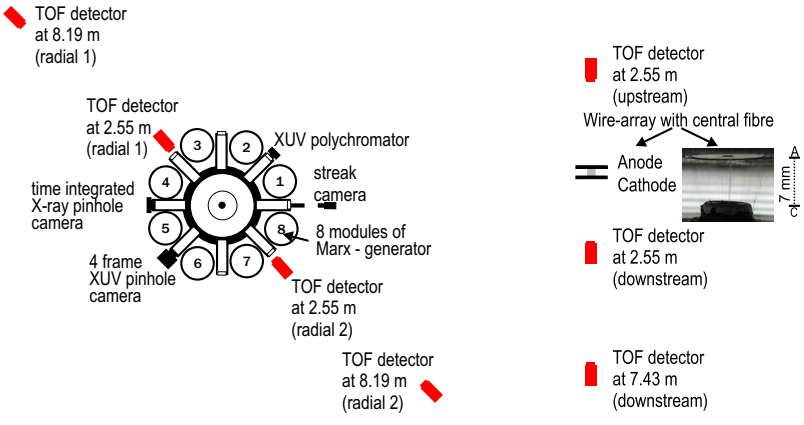

FIG. 2. (Color online) A schematic diagram of our diagnostic setup with seven time-of-flight neutron detectors.

axis. The plasma 3 mm away from the cathode was imaged on the slit of the streak camera.

(ii) A time-integrated pinhole camera was differentially filtered (without a filter, and with 5 and 24 μm Mylar).

(iii) A gated pinhole camera recorded four frames with 2 ns exposure and 5 or 10 ns interframe separation.

(iv) A time-resolved soft-x-ray polychromator was used for the estimation of radiated energy and also for the measurement of spectral power density in various spectral channels.

(v) Seven scintillators and photomultiplier tubes enabled the TOF analysis of fusion neutrons. Three axial (end-on) neutron detectors were located at distances of −2.55 m (the minus sign means upstream, i.e., behind the anode), 2.55 m, and 7.43 m (downstream, behind the cathode). Four radial (side-on) detectors were positioned in a row at distances of −8.19, −2.55, 2.55, and 8.19 m from the Z-pinch plasma. To prevent hard x rays from saturating photomultipliers, detectors were shielded by 5–10 centimeters of lead. The detector time resolution of about 4 and 7 ns was given mainly by the decay time of scintillators, by the rise-time of the photomultiplier tube, and by a neutron transit time through 5 and 10 cm thick scintillators, respectively. The time resolution of neutron detection was further strongly influenced by the detector distance from the neutron source. For example, at the distance of 2.55 m, the instant neutron emission was broadened to 7 ns in the case of the neutron energy spectrum with 2.45 MeV peak and 300 keV full width at half-maximum (FWHM). Because it was possible to distinguish two neutron peaks 11 ns apart from each other, the experimentally estimated temporal resolution of neutron detection was about 10 ns.

(vi) The neutron yield was measured with the use of an indium activation counter and thermoluminescent dosimeters.

(vii) High-voltage and dI/dt probes provided information about electrical characteristics and the power input into the discharge.

This set of diagnostic tools enabled us to observe results that are presented in the following section. All times described in this paper refer to the start of a current when $t=0$. All signals were adjusted to account for different transit times from each detector to oscilloscopes. The temporal uncertainty between waveforms of soft x rays, hard x rays, neutrons, and electrical characteristics was below 5 ns.

IV. EXPERIMENTAL RESULTS

In order to describe Z-pinch discharges that show specific experimental results in each shot, it is important to use simultaneously comprehensive diagnostics with temporal, spatial, and spectral resolution. For this reason, we illustrate the most important results on carefully chosen individual shots that most evidently describe general characteristics of the experiment.

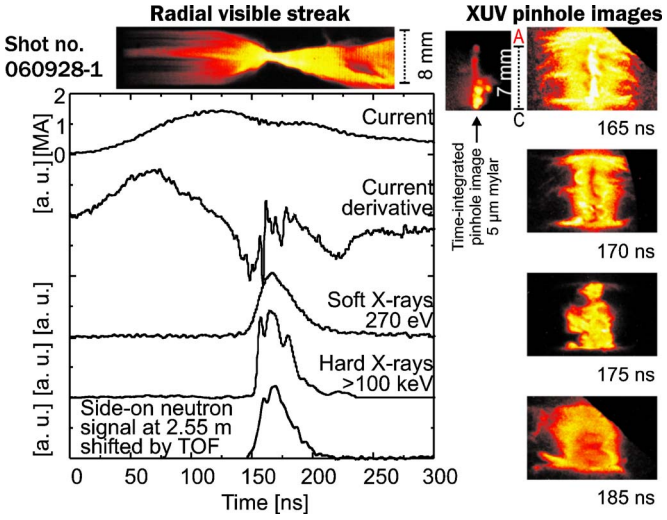

FIG. 3. (Color online) A visible streak image, XUV pinhole images and waveforms of current, current derivative, soft x rays, hard x rays, and neutron emission recorded in Discharge No. 060928-1, with a neutron yield of about 9×10^8. Note: The detection efficiency varied between frames of the XUV pinhole camera.

Figure 3 presents typical results of the implosion of the conical tungsten wire array onto the deuterated polyethylene fiber. Evidently, the streak image shows the radiation from the fiber and/or precursor plasma already at 50 ns. At about 130 ns, the tungsten wire array started to implode with the velocity approaching the value of 2×10^5 m/s. The most intense soft x rays were emitted near the cathode at about 160 ns during the stagnation of imploded tungsten wires onto the $(CD_2)_n$ fiber. The power of soft x rays (above 100 eV) reached 100 GW. The total emitted energy was about 5 kJ. The maximum spectral power density of about 0.5 GW/eV was measured at a photon energy of 120 eV. The radiation was close to the radiation of a black body with a temperature of 40 eV.

Hard-x-ray emission started at the final stage of the wire array implosion. The rise time of a hard-x-ray signal was very short and usually did not exceed 3 ns. In all shots, the onset of x-ray emission corresponded to a dip in the dI/dt signal. After that, the hard-x-ray emission lasted for about 30 ns, i.e., during the stagnation and expansion phase.

As far as neutron emission is concerned, it temporally correlated with hard x rays within 5 ns accuracy. The neutron pulse lasted on average 30 ± 5 ns (FWHM). In Fig. 4, we can see the neutron spectrum obtained perpendicularly to the Z-pinch axis. In this particular shot, the peak neutron energy detected in the side-on direction was slightly shifted from 2.45 MeV. On average, the peak neutron energy was 2.48 ± 0.05 MeV and the FWHM of neutron energy spectra was 450 ± 100 keV. As regards the axial direction [see Fig. 4(c)], the energy of neutrons detected downstream was always above 2.45 MeV. When we calculated the average downstream neutron energy spectrum from 15 shots, it peaked at 2.65 ± 0.10 MeV with 350 ± 100 keV FWHM.

The knowledge of neutron spectra at different directions relative to the Z-pinch axis carries important information about the energy of deuterons that produce fusion reactions.

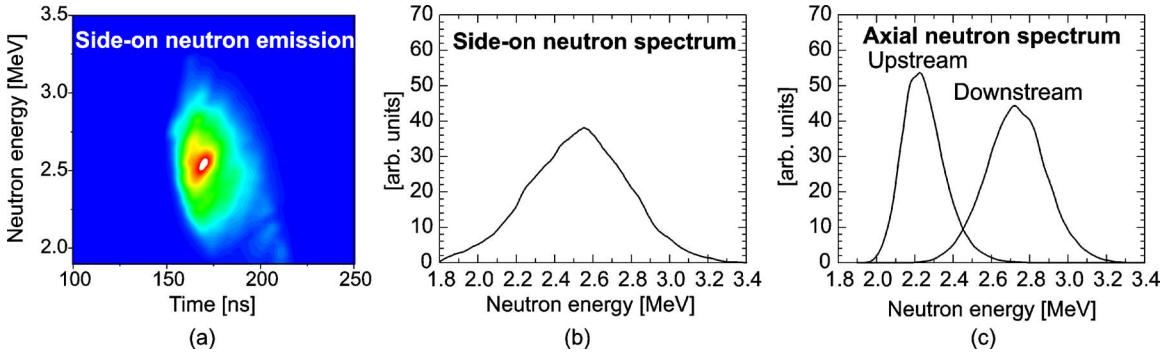

FIG. 4. (Color online) (a) and (b) Side-on neutron emission time and neutron energy spectrum. (c) Axial neutron energy spectrum, Shot No. 060928-1.

Assuming a binary reaction of a fast deuteron with a stationary one, the neutron energy E_n depends on the deuteron energy E_d and on the laboratory angle between the colliding fast deuteron and the outgoing neutron θ as

$$E_n(E_d,\theta) = E_d \frac{m_n}{2(m_n+m_{He})} \cdot \left(\cos\theta + \sqrt{\frac{m_{He}}{m_n}\left(1+\frac{2Q}{E_d}\right) - \sin^2\theta}\right)^2, \quad (2)$$

where $Q \doteq 3.27$ MeV is the energy released from D–D fusion reactions, m_n is the neutron mass, and m_{He} is the mass of helium. It follows from this equation that it is necessary to know the angle θ in order to estimate the deuteron energy from the neutron energy. Fortunately, if the deuteron energy E_d is much smaller than the fusion energy Q, we obtain

$$E_n(E_d,\theta) \approx E_d \frac{m_n}{2(m_n+m_{He})} \cdot \left(\cos\theta + \sqrt{\frac{m_{He}}{m_n}\cdot\frac{2Q}{E_d}}\right)^2, \quad (3)$$

$$E_n(E_d,\theta) \approx g(E_d\cos^2\theta) + \frac{m_{He}}{m_n+m_{He}}\cdot Q \doteq g(E_d\cos^2\theta) + 2.45\ \text{MeV}. \quad (4)$$

Then the neutron energy E_n is only a function of the component of the deuteron kinetic energy in the direction of neutron detection $g(E_d\cos^2\theta)$.

On the basis of Eq. (4), it was possible to transform neutron energy spectra into distribution functions of side-on and end-on energy components of deuterons (see Fig. 5). The divergence around small deuteron energies in Fig. 5 is given by a large dE_n/dE_d near 2.45 MeV neutron energy (cf. Fig. 1).

In Fig. 5, we can see that neutrons were produced mainly by deuterons with a kinetic energy component below 100 keV. The mean axial component of the deuteron kinetic energy $\langle|E_\parallel|\rangle$ was 60 keV while the mean side-on component $\langle|E_\perp|\rangle$ was 40 keV. Therefore, the average kinetic energy of reacting deuterons was $\langle E_d\rangle = \langle E_\parallel\rangle + 2\langle|E_\perp|\rangle \doteq 150$ keV. Our Monte Carlo reconstruction also estimated the downstream/upstream anisotropy of neutron flux as 1.2.

In Shot No. 060928-1, there were only a few downstream neutrons below 2.45 MeV and thus most of the deuterons were directed toward the cathode. In some other shots, a different case occurred. Figure 6 shows results from Shot No. 060922-2, in which the same number of neutrons as in Shot No. 060928-1 was detected. In this particular shot it is also evident that neutrons were emitted together with hard and soft x rays. In addition to that, the neutron emission temporally correlated with the voltage rise up to 400 kV. As regards distribution functions of neutron and deuteron energy, they are displayed in Fig. 7. In comparison with Shot No. 060928-1, neutron and deuteron energy distribution functions were more isotropic. The mean neutron energy observed downstream was about 2.55 MeV. According to our calculation, the side-on and end-on neutron spectra imply the neutron flux anisotropy below 1.2.

A. Correlation of neutron emission with hard x rays and electrical characteristics

Figures 3 and 6 show how neutron emission temporally correlated with hard x rays. Because the Monte Carlo reconstruction could blur a real neutron signal, we displayed the waveform of the nearest side-on neutron detector to obtain more accurate values of the shift between hard-x-ray and neutron emission. In Fig. 8(a), we can see how neutron emission correlated with hard x rays with a small delay, which

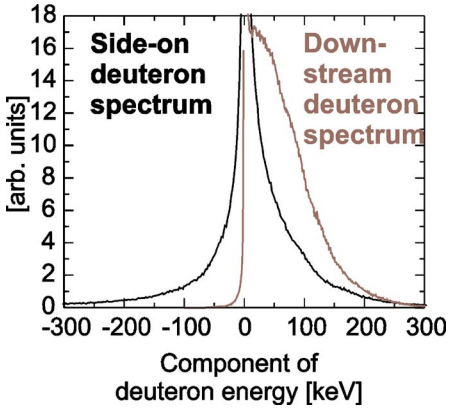

FIG. 5. (Color online) Distribution functions of the kinetic energy component of deuterons that produced fusion neutrons, Shot No. 060928-1. (The energy distribution function of all deuterons was not obtained because the assumption of a thin target is not valid and therefore it is not sufficient to include the fusion cross section and the stopping power into the calculation. One has to include also the slowing-down of fast deuterons.)

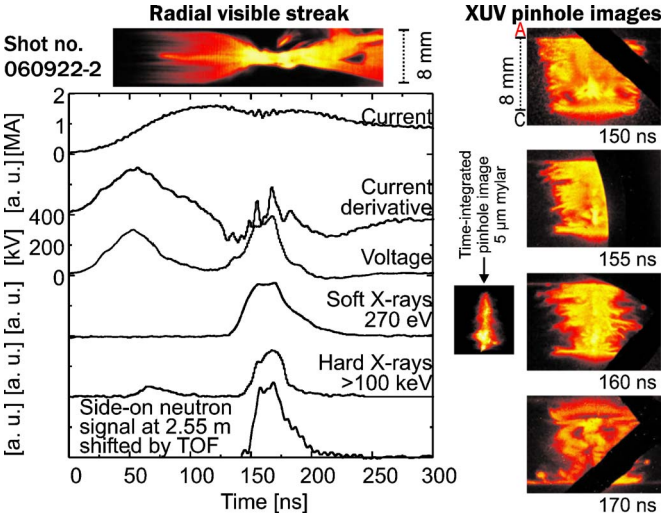

FIG. 6. (Color online) A visible streak image, XUV pinhole images and waveforms of current, current derivative, voltage, soft x rays, hard x rays, and neutron emission recorded in Discharge No. 060922-2, with a neutron yield of about 9×10^8.

was about 4 ns. A part of this delay could be attributed to the transit time of neutrons through the TOF detector and to the uncertainty of neutron energy estimation.

As regards measured voltage, there was also a strong correlation with side-on and end-on neutron emission. An exemplary result can be seen in Fig. 8(b).

Another common feature of our experiment was the rapid rise of hard-x-ray and neutron emission after the dip in the dI/dt signal. After this dip, the current derivative oscillated for about 50 ns and during this period neutrons and hard x rays were detected. It was clear that neutron emission correlated with dI/dt peaks rather than with minima [see Fig. 8(c)] and that the induced voltage $L\mathrm{d}I/\mathrm{d}t$ contributed to voltage peaks [see Fig. 8(d)].

On the basis of voltage V, current I, and dI/dt measurements, it was possible to calculate the plasma resistance R_P and time-varying inductance $\dot{L}_P$ from the equation

$$R_P+\dot{L}_P=\frac{V-L\dot{I}}{I}, \tag{5}$$

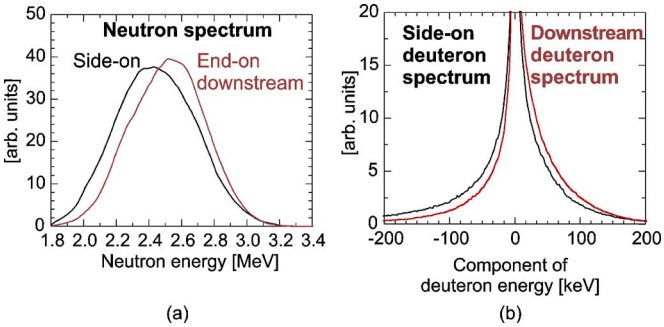

FIG. 7. (Color online) (a) Side-on and end-on energy spectra of neutrons. (b) Distribution functions of the kinetic energy component of reacting deuterons, Shot No. 060922-2.

where $L(t)=L_P(t)+L_0$ is the inductance including the external inductance of transmission line L_0. We assumed that the inductance $L(t)$ of about 9 nH was approximately constant during the implosion. But results would not change qualitatively even if we calculated with the increased inductance of about 14 nH. The results of the $R_P+\dot{L}_P$ term from shots No. 060922-2 and No. 060921-1 are displayed together with neutron emission and a streak image in Fig. 9. In each shot, the neutron emission started at the end of the wire array implosion and lasted for about 40 ns up to the expansion phase. During this period, the energy input $\int(R_P+\dot{L}_P)I^2\mathrm{d}t$ approached 20 kJ.

B. Neutron yield

The study of neutron generation in our experiments at the S-300 generator was focused mainly on the estimation of emission time and neutron energies. The neutron yield was estimated from one indium activation detector assuming the 4π isotropy. Values of neutron yields are therefore important mainly for a relative comparison of individual shots. In this respect, we wanted to know whether the neutron yield was dependent on any parameter of the Z-pinch discharge. The only parameter that we recognized that played some role was the peak of an electric current. Figure 10 shows the scaling of the neutron yield with the magnitude of an electric current. The average neutron yield from 15 shots was 6×10^8 while the peak neutron yield reached the value of 10^9 for 1.65 MA current.

In order to improve neutron yield measurements, we tried to use thermoluminescent dosimeters (TLDs), which were placed inside a 10–in.-thick Bonner sphere, 1 m from the neutron source (cf. Ref. 38). As regards the experiments described in this paper, neutron signals from TLDs were overlaid by a strong hard-x-ray background. In preliminary deuterium gas-puff experiments in which hard x rays were less intensive in comparison with neutron emission, results from TLDs were used for cross-calibration of our indium activation detector *in situ*. According to this cross-calibration, there was an indication that our indium activation detector underestimated neutron yields. We are going to pay more attention to the absolute measurement of neutron yields in future experimental campaigns.

C. Comparison with cylindrical wire array imploding onto deuterated fiber

In this subsection, we present results from the implosion of standard cylindrical tungsten wire arrays onto a fiber as we believe it is valuable to compare the experiment with conical wire arrays with other configurations with similar initial parameters. In the following subsection, we also show results from shots when only a fiber without any imploding wire array was used.

The experimental series with standard tungsten wire-arrays consisted of 17 shots whereas the series with conical wire arrays consisted of 15 shots. We present more detailed results from conical wire array experiments in this paper

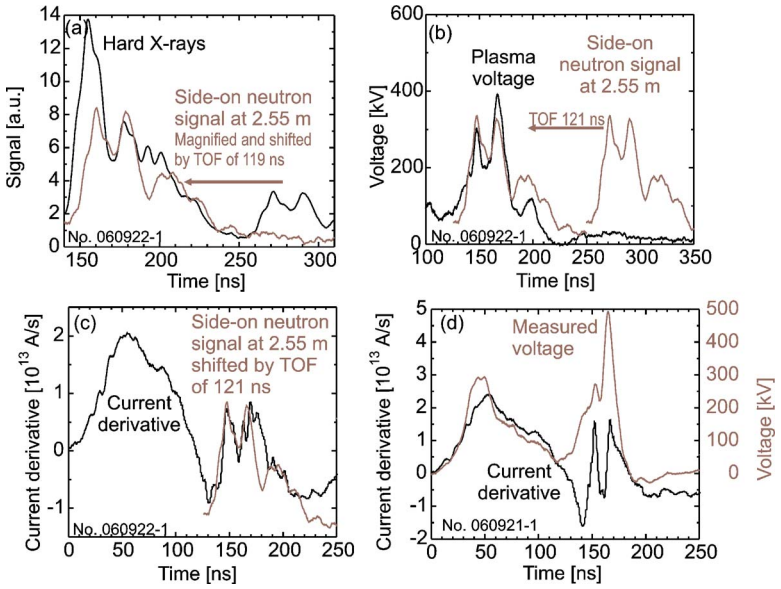

FIG. 8. (Color online) (a)–(c) Examples of the correlation of hard x rays, plasma voltage, and dI/dt signal with neutron emission at the side-on detector in Shot No. 060922-1. 120 ns represents the time-of-flight of 2.4 MeV neutrons to the detector located at 2.55 m. (d) An example of plasma voltage and current dI/dt measured in Shot No. 060921-1.

because diagnostics of cylindrical wire arrays consisted of a lower number of neutron detectors. In the case of the standard wire array, 40 tungsten wires of 5 μm diameter and 10 mm length were used. As far as the conical wire array is concerned, it consisted of 30 tungsten wires of 7 μm diameter and 7 mm length. Both experiments were carried out on the same current generator with similar deuterated fibers and similar currents of about 2 MA.

Also experimental results demonstrated a lot of similarities. The average neutron yield from a standard wire array was about 9×10^8. Thus the neutron yield per length was similar to the one presented above for conical wire arrays. Statistical data from cylindrical and conical wire arrays showed that differences in neutron emission time and neutron spectra were smaller than the shot to shot variation. As an example, we chose the shot displayed in Fig. 11. We would like to present this shot in order to demonstrate that neutrons were emitted after 180 ns, i.e., during the plasma expansion. These features were not so obvious in all shots, but late or delayed neutron emission was observed in the case of conical wire arrays as well.

D. Comparison with fiber Z pinch

During the experimental series with standard tungsten wire arrays, we also tried to initiate the Z pinch from one deuterated fiber only, i.e., without any wire array. Such an experiment seemed to be interesting for comparing our results with those obtained in the 1970s and 1980s.[12,15–17] The average neutron yield of about 1×10^8 was several times lower than in our experiments with the implosion of a wire array onto a fiber. The typical results that we obtained are displayed in Fig. 12. From these images, it can be clearly seen how $m=0$ unstable plasma was expanding from the very beginning of the current. The neutron emission was triggered at about 70 ns and lasted for a relatively long time of more than 60 ns. At this point, it should be said that hard-x-ray and neutron signals in Fig. 12 were taken from the same waveform recorded by the TOF detector at 2.55 m. The temporal uncertainty given by the spread of neutron energies was below 5 ns. This means that there was a real delay between the neutron production and the hard-x-ray emission. Figure 12 shows that the peak neutron energy in the axial (down-

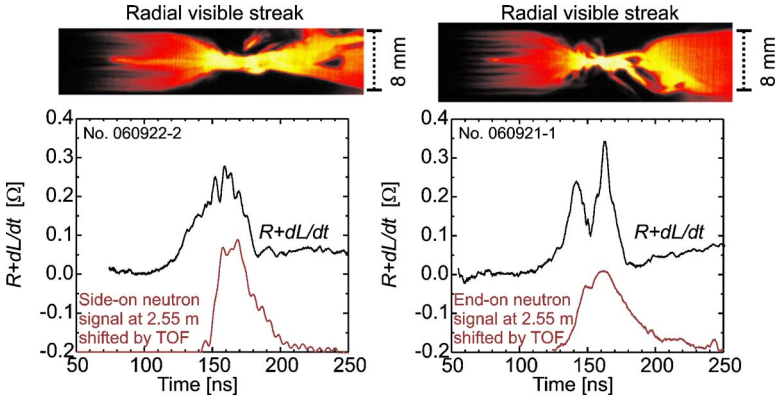

FIG. 9. (Color online) The plasma impedance $R_P+\dot{L}_P$, neutron emission, and streak images in shots No. 060922-2 and No. 060921-1.

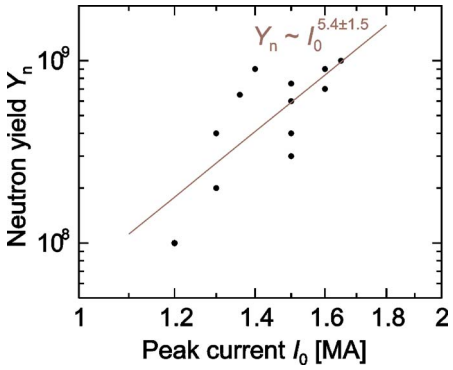

FIG. 10. (Color online) Neutron yield scaling with the current. The conical tungsten wire array imploding onto a deuterated polyethylene fiber.

stream) direction was about 2.65 MeV. Whereas the plasma dynamics and the neutron emission time completely differed from the ones obtained with an imploding wire array, the neutron spectra were very similar (cf. Fig. 12 with Fig. 7). In addition to that, similar spectra were acquired also in our preliminary experiments with a deuterium gas-puff.

V. DISCUSSION OF NEUTRON PRODUCTION MECHANISM

During the past 60 years, plasma theory and modeling were improved to such a degree that it was possible to explain gross dynamics of the discharge as well as a lot of "fine" phenomena of Z pinches. However, several crucial issues such as the mechanism of neutron production have remained unresolved. A recent review on the generation of fast particles was given by Ryutov *et al.*,[39] Haines,[40] and Vikhrev and Korolev.[21] In plasma foci, a lot of experimental results have been obtained and also the neutron production mechanism has been studied up to the present time (see Ref. 41 and references therein). In this respect, experimental data from Z pinches are more rare.

A. Neutron emission anisotropy and beam-target model

Measurements of neutron energies and neutron emission time play an important role in the discussion of the neutron production mechanism. As regards experiments on the S-300 generator, the peak neutron energy detected downstream was shifted from 2.45 MeV toward higher energies in all shots. One could therefore think that a deuteron beam was accelerated toward the anode. However, a small shift above 2.45 MeV could also be a result of significant kinetic energies of fast deuterons (e.g., in a very high-temperature plasma). To exclude this, it was favorable to use neutron detectors also in the upstream axial direction. In our case, upstream neutron energies were smaller than downstream ones. That is why most fusion reactions were realized in the center-of-mass frame, which was moving with respect to the laboratory frame of reference.

Of course, there is still a possibility of a thermonuclear source moving toward the cathode, a so-called moving thermonuclear boiler. But the observed shift to 2.7 MeV [cf. Fig. 4(c)] requires the unreasonable high velocity of about 2×10^8 cm/s toward the cathode. In addition to that, we used such an orientation of the conical wire array that the zippering occurred in the opposite direction, i.e., toward the anode (see Fig. 3). This result indicated that the neutron emission anisotropy was caused by a beam of fast deuterons that were directed toward the cathode and which were colliding with "cold" target deuterons. At this point, we should mention that the neutron emission could be strongly influenced not only by the anisotropic energy distribution function of fast deuterons but also by an inhomogeneous density of target deuterons.

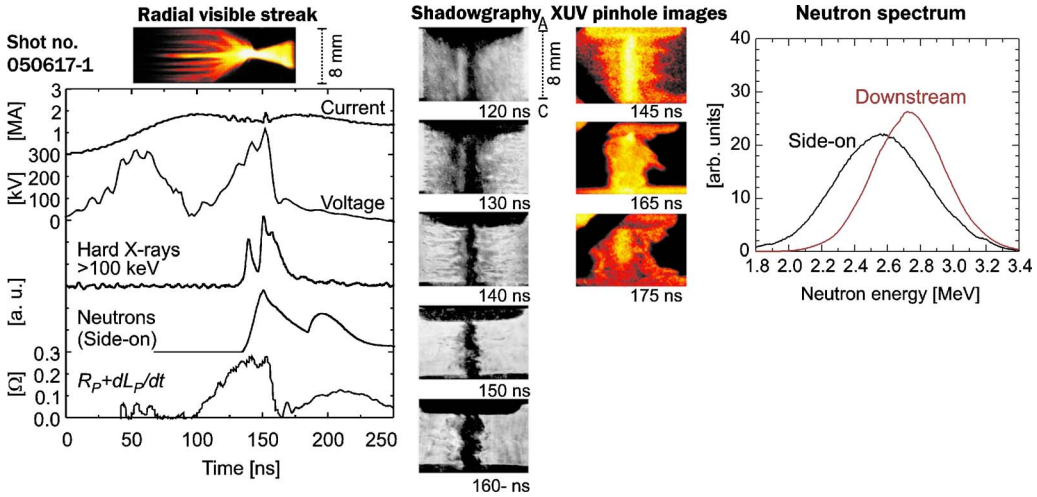

FIG. 11. (Color online) A visible streak image, an XUV pinhole image, shadow images, neutron energy spectra and waveforms of current, voltage, hard x rays, and neutron emission time recorded with the standard tungsten wire array imploding onto a deuterated fiber. Shot No. 050617-1, a neutron yield of about 2.5×10^9.

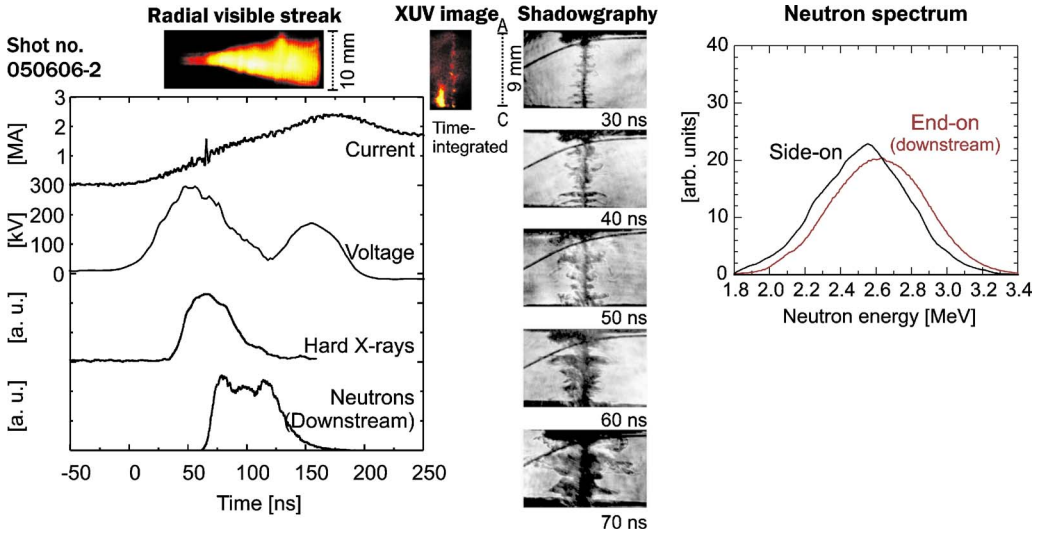

FIG. 12. (Color online) A visible streak image, an XUV pinhole image, shadow images, neutron energy spectra and waveforms of current, voltage, hard x rays, and neutron emission time recorded without an imploding wire array, i.e., only with the deuterated fiber of 100 μm diameter. Shot No. 050606-2, a neutron yield of about 4×10^8.

B. Radial energy component of deuterons and the generalized beam-target model

So far we have discussed results from axial neutron detectors. As regards the side-on direction, an important result is the 450 keV FWHM of neutron energy spectra. Almost the same value was observed in our experiments with a standard wire array (see Fig. 11) or with a fiber (see Fig. 12) as well as in other Z-pinch configurations (gas-embedded Z pinch,[3–5] gas-puff Z pinch,[22] and plasma focus[42,43]). Such a broad width of neutron spectra implies high radial velocity of deuterons. Figures 5 and 7 show that the side-on component of deuteron kinetic energy is comparable with the axial one. It might be a result of magnetic and/or electric fields in Z pinches.

As regards the influence of electric fields, a large component of velocity in all directions could be achieved for instance in a turbulent plasma. If this is not the case, trajectories of deuterons accelerated axially could be curved by magnetic fields. The influence of magnetic field can be evaluated by the ratio between the Larmor r_{Larmor} and pinch radius R. For a deuteron with the kinetic energy E_{d}, the mass m_{d}, the charge e in the magnetic field B produced by the cylindrical current I, the ratio r_{Larmor}/R is given by

$$\frac{r_{\mathrm{Larmor}}}{R}=\frac{m_{\mathrm{d}}\sqrt{2E_{\mathrm{d}}/m_{\mathrm{d}}}}{eBR}=\frac{2\pi\sqrt{2E_{\mathrm{d}}m_{\mathrm{d}}}}{e\mu_0 I}\approx\frac{\sqrt{E_{\mathrm{d}}[\mathrm{MeV}]}}{I[\mathrm{MA}]}. \quad (6)$$

For the deuteron energy $E_{\mathrm{d}}=150$ keV and the current $I=1.5$ MA, we obtain the ratio $r_{\mathrm{Larmor}}/R\approx0.25$, which means that fast deuterons could be confined by the magnetic field within the pinch diameter. In such a case, the classical linear beam target model does not occur. Instead of the rectilinear motion, trajectories of fast deuterons could be rather complex. If we simplify trajectories, deuterons can move similarly as described earlier by Bernstein and Comisar.[42] Such curved trajectories of deuterons could explain not only the observed neutron spectra but also the neutron flux anisotropy. It is known that the neutron emission probability is highly anisotropic at high deuteron energies [cf. Fig. 1(b)]. In the case of the classical rectilinear beam target model, the neutron flux ratio $Y_{\theta_1}/Y_{\theta_2}$ for $\theta_1=0°$ and $\theta_2=90°$ is 2.5 for 150 keV deuterons. If we take into account curved trajectories, however, the flux anisotropy can be substantially decreased. This is probably the reason why the neutron flux anisotropy in most Z-pinch[17,23,24,44] and plasma focus[42,45] experiments was below 1.7.

C. Stopping power and number of accelerated deuterons

Another parameter that determines trajectories of deuterons is the stopping power of fast deuterons. According to Ref. 46, the Coulomb energy loss of fast deuterons E_{d} in a plasma target of the length x could be expressed as

$$\frac{dE_{\mathrm{d}}}{dx}=\frac{n_{\mathrm{bound}}}{n_{\mathrm{bound}}+n_{\mathrm{free}}}\left(\frac{dE_{\mathrm{d}}}{dx}\right)_{\mathrm{cold}}+\frac{n_{\mathrm{free}}}{n_{\mathrm{bound}}+n_{\mathrm{free}}}\left(\frac{dE_{\mathrm{d}}}{dx}\right)_{\mathrm{free}}+\left(\frac{dE_{\mathrm{d}}}{dx}\right)_{\mathrm{ions}}, \quad (7)$$

where n_{bound} and n_{free} represent the density of bound and free electrons, respectively. If we assume homogeneously mixed ions in a stagnated Z pinch and the ratio $n_{\mathrm{bound}}/(n_{\mathrm{bound}}+n_{\mathrm{free}})$ above 1/2, fast deuterons are decelerated mainly by electrons bounded in tungsten ions. This means that

$$\frac{dE_{\mathrm{d}}}{dx}\approx\frac{n_{\mathrm{bound}}}{n_{\mathrm{bound}}+n_{\mathrm{free}}}\left(\frac{dE_{\mathrm{d}}}{dx}\right)_{\mathrm{cold}}\geq\frac{1}{2}\left(\frac{dE_{\mathrm{d}}}{dx}\right)_{\mathrm{cold}}. \quad (8)$$

In the case of 30 tungsten wires of 7 μm diameter and the plasma diameter of about 2 mm, the density of tungsten ions is estimated as 2×10^{19} cm^{-3}. For a 150 keV deuteron, the stopping power $\frac{1}{2}(dE_{\mathrm{d}}/dx)_{\mathrm{cold}}$ calculated with SRIM tables[47] is $\approx$50 keV/mm and the deuteron is decelerated on the length l_{free} of the order of 3 mm.

The number of accelerated deuterons N_d depends on the neutron yield N_n, the D–D fusion cross section $\sigma_{fusion}(E_d)$, the deuteron density n_d, and the length l_{free} as

$$N_d = \frac{N_n}{\sigma_{fusion}(E_d) n_d l_{free}}. \quad (9)$$

For the neutron yield $N_n = 10^9$, the fusion cross section $\sigma_{fusion}(150\ \text{keV}) = 2.8 \times 10^{-30}\ \text{m}^{-2}$ (see Ref. 34), the deuteron density $n_d \approx 10^{20}\ \text{cm}^{-3}$, and the length $l_{free} = 3 \times 10^{-3}$ m, we obtain the number of accelerated deuterons $N_d \approx 10^{15}$.

D. Acceleration mechanisms

When we talk about the neutron production mechanism here, we mean the way deuterons are accelerated. We showed in previous paragraphs that the generalized beam-target model played an important role in our wire array and also fiber Z-pinch experiments. However, it is still not clear how the beam of fast deuterons was created. To discuss this issue, we must look at waveforms of plasma voltage, current, and current derivative.

1. Acceleration by induced electric fields

An obvious result of our experiment was the correlation of 400–500 kV voltage peaks with neutron emission (see Fig. 8). Therefore, it seems reasonable to explain the deuteron acceleration to 150 keV energies by diode action. Also one of the first explanations in the 1950s suggested that charged particles in Z pinches were accelerated by the diode action in a large induced voltage. The observed induced voltage was ascribed to a large increase of the inductance $\dot{L}_P > 0$, which resulted from the growth of instabilities[4] or from the collapsing of the main plasma column.[48] The question we should ask here is what electric field $\vec{E}$ occurs in the plasma? Even though the voltage peak across the plasma is measured, it is not clear that a high electric field is also seen by deuterons. In the presence of time-varying magnetic fields, it cannot be assumed that the measured voltage is given only by the integration of the axial electric field E_z along the length of a plasma column. Besides that, as has already been pointed out,[49] the electric field seen by ions in an imploding plasma is $\vec{E} + \vec{v} \times \vec{B} = 0$.

The drawback of the acceleration model described above is its limitation on the imploding plasma. As regards our results, we observed similar phenomena as other researchers in many Z-pinch and plasma focus experiments (see, for instance, Refs. 5, 44, and 50–53): neutrons were generated mainly after the plasma implosion during the stagnation and during the global plasma expansion when the dI/dt signal was rising. That is, for example, why Trubnikov[54] and Uhm[55] extended the acceleration mechanism based on induced fields also for the plasma expansion. Trubnikov considered a rapid transfer of a current to a peripheral plasma. A high transient electric field then accelerates deuterons that are not coiled by the magnetic field. Because it is necessary to explain high radial velocities of deuterons, axially accelerated deuterons have to be bent by magnetic fields before they produce fusion neutrons. Another issue that should be discussed here is the negative value of induced voltage $\dot{L}_P I$ during the expansion.

2. Role of microturbulence and enhanced resistance

A more realistic approach was considered by the authors in Refs. 40, 42, 44, 51, and 56. Even though there are differences in argumentation, all these authors emphasized the role of microturbulence and anomalous resistance during the plasma stagnation and expansion. The role of microturbulence lies in the fact that it can cause rapid magnetic field diffusion and fast current redistribution. Then, a large $\partial \vec{B}/\partial t$ could accelerate ions in one direction near the axis and in the opposite direction in the peripheral plasma. Besides, microturbulence could not only generate induced electric fields but also form a high-energy tail of the ion distribution function.[39,57] From an experimental point of view, the onset of microinstabilities just before neutron emission was clearly shown by Bernard *et al.* with laser scattering in a plasma focus discharge.[43] The measured plasma resistance during the plasma stagnation exceeded the Spitzer value and reached 0.2–0.4 Ω for a broad energy range of plasma focus machines.[56,57]

As regards our experiment, we measured the $(R_P + \dot{L}_P)$ term (see Fig. 9). On the one hand, the measured value of about 0.2–0.4 Ω during the implosion could be ascribed to a time-varying inductance. Then the energy would be naturally coupled from the generator through the $\dot{L}_P$ term. But on the other hand, it is impossible to explain a 40 ns duration of 0.2 Ω by a constantly increasing plasma inductance only. If the plasma resistance is neglected, there is no evidence of the plasma expansion and the total increase of inductance $\Delta L_P = \int \dot{L}_P dt$ is about 10 nH. Such an inductance increase of the 7 mm long plasma column requires the collapse to a 10 μm diameter. A more likely explanation of the inductance rise is the increase of the effective plasma length. This might be a result of complex helical structures that develop usually after the stagnation.[58] However, the main argument against neglecting plasma resistance is that the magnetic energy $\frac{1}{2}\Delta L_P I^2 \doteq 10$ kJ could be hardly stored at the time when the plasma column expanded to a few millimeter diameter and when a significant fraction of the energy had already emitted from the plasma. This led us to a conclusion that the influence of resistive heating during the stagnation was growing. For the Spitzer resistance and for experimentally estimated values during the stagnation (plasma radius $R = 1$ mm, length $l = 5 \times 10^{-3}$ m, electron temperature $kT_e = 50$ eV, effective charge $\bar{z} = 10$, and Coulomb logarithm $\ln \Lambda \doteq 10$), we get

$$R_P \doteq \frac{10^{-4} \bar{z} \ln \Lambda}{kT_e^{3/2}} \cdot \frac{l}{\pi R^2} \doteq 0.05\ \Omega.$$

Since the result comes out less than 0.2 Ω, the classical Spitzer resistivity is also insufficient to explain the measured value of the plasma impedance.

Here, the research of neutron emission is related to the energy conservation, which has recently become a debated issue in wire-array Z pinches (see, e.g., Refs. 27, 58, and 59).

Already 25 years ago, however, Riordan *et al.* pointed out that the observed radiation yield was significantly higher than the kinetic energy input.[60] From that time on, several models have been suggested to explain the observed discrepancy. In this respect, the enhanced resistance was considered as an explanation, for instance, by Whitney with his colleagues in Saturn experiments.[61] On the MAGPIE generator, Chittenden explained the enhancement of ohmic heating by the onset of $m=1$ instabilities after the secondary implosion of trailing mass.[62]

3. Thermonuclear neutrons

Our experiments demonstrated the strong correlation between neutron emission and measured plasma voltage. The question that still remains is whether the acceleration mechanism is connected with a high voltage induced across a plasma column (see Sec. V D 1), or with ion acceleration in microturbulence (see Sec. V D 2), or with the power input into a plasma. The process mentioned last is closely related to the thermonuclear origin of neutrons and it was explored mainly by Vikhrev in Refs. 21, 63, and 64. The adiabatic heating in necks of $m=0$ instabilities was considered also by Young *et al.* in experiments with deuterated polyethylene fibers of >50 μm diameter.[17] Riley and colleagues pointed out that it is impossible to interpret neutron measurements in fiber Z pinches if the ion temperature equals the electron temperature. Instead of it, they explained observed neutron yields by the direct heating of ions within turbulence arising from instability growth.[65] Recently, the ion temperature higher than the temperature of electrons was assumed by Velikhovich *et al.* in the calculation of thermonuclear yields in a deuterium gas-puff.[23]

From the experimental point of view, thermonuclear D–D fusion reactions in the center-of-mass frame of reference are characterized by isotropic neutron emission and by a mean neutron energy of about 2.45 MeV. It is evident from Figs. 4(b) and 4(c) that most of the neutrons in our experiments came from the beam-target interaction. However, it is still possible that the beam originated from a Maxwellian plasma or from another isotropic ion energy distribution. For example, the beam of fast deuterons could be accelerated within a high-temperature plasma and afterwards it escaped and penetrated through a low-temperature plasma where fusion neutrons were produced. Consequently, the observed neutron emission anisotropy could be a result of strong magnetic and electric fields[21,64] as well as a result of anisotropy of target deuterons. In all cases, however, a broad neutron energy spectrum requires a relatively high temperature. According to the equation $\Delta E_{\mathrm{d}}(\mathrm{keV})=82.5\sqrt{kT_{\mathrm{i}}[\mathrm{keV}]}$ (e.g., Ref. 28), the width of a neutron spectrum $\Delta E_{\mathrm{d}}=500$ keV corresponds to the equivalent ion temperature $kT_i \approx 30$ keV. Such a high temperature could be achieved locally in a small volume, otherwise the neutron yield would be much higher. In our experiment, for instance, if we assume that the neutron yield of 10^9 was thermonuclear and originated from the bulk of plasma, we obtain plasma temperatures of about 2 and 100 keV width of a neutron spectrum.

But even though we admitted that a fraction of fast deuterons was accelerated by elastic collisions in a high-temperature locality, it could not be referred to as thermonuclear fusion and also it would not be useful for energy production. If deuterons escape a high-temperature region, they are slowed down by cold deuterons usually without undergoing fusion reactions. The fusion energy released is always smaller than the energy expended on the acceleration of fast deuterons. The only way how to achieve the energy gain is to transfer the lost energy of fast deuterons to the acceleration of other deuterons in the same plasma, i.e., to achieve the energy feedback. For that purpose, it is necessary to keep fast deuterons in a high-temperature region or to use fast deuterons for heating of a surrounding plasma to a fusion temperature. As regards Z pinches, a magnetic field seems to have the crucial importance in prevention of fast deuterons from escaping a plasma.

At this point, we would like to go back to the discussion of the model of deuteron acceleration. The problem of the acceleration mechanism is that it should clarify not only the observed peak value of plasma voltage but also a comparatively long duration of neutron emission. On the one hand, there does not seem to be a problem to ascribe 400 kV voltage peaks to a large rise of the inductance dL_P/dt, the current rise dI/dt, and the resistance R_P. But on the other hand, it is necessary to elucidate up to 40 ns long neutron emission at the post-stagnation phase. We believe that the acceleration mechanism in a turbulent plasma perhaps fits best to a prolonged neutron emission and to broad side-on neutron spectra. The onset of microturbulence then could induce high plasma voltage as well as form a high-energy tail in deuteron velocity distribution. Nevertheless, the origin of microturbulence and a more detailed description of the acceleration mechanism are beyond our possibilities of experimental data interpretation. However unclear this issue may be, it holds that the research of the neutron origin is connected with the study of plasma voltage and with the power input into a plasma. It follows that the acceleration is connected with the global plasma dynamics and that the deuteron acceleration is not a "secondary" process in plasma.

VI. CONCLUSION

The implosion of a conical wire array Z pinch onto a deuterated polyethylene fiber was studied on the S-300 pulsed power generator at the Kurchatov Institute. The study of neutron emission in these experiments was focused mainly on the estimation of neutron energies and neutron emission time. The neutron measurement was used to obtain significant data about acceleration of fast ions in Z-pinch plasmas.

First, as regards neutron energies in the side-on direction, the neutron energy spectrum peaked at 2.48 ± 0.05 MeV with 450 ± 100 keV FWHM. In the downstream direction, the peak neutron energy and the width of a neutron spectrum were 2.65 ± 0.10 MeV and 350 ± 100 keV, respectively. The knowledge of neutron spectra at different directions relative to the Z-pinch axis provided information about the energy of deuterons that produced fusion reactions.

The average kinetic energy of reacting deuterons was about 150 keV. Most of the deuterons were directed toward the cathode. The broad width of neutron spectra implied a high radial velocity of deuterons. Therefore, trajectories of deuterons producing fusion reactions seemed to be strongly influenced by magnetic and/or turbulent electric fields. This observation was made also in experiments with an imploding standard wire array as well as in fiber Z pinch.

Moving to the second subject of our interest, i.e., neutron emission time, the neutron pulse temporally correlated with hard x rays and also with measured voltage. The neutron emission lasted on average 30 ± 5 ns (FWHM) and was observed at the end of implosion and during the expansion of a plasma column. At this moment, the $R_P + \dot{L}_P$ term reached $0.2-0.4\ \Omega$. During the implosion, this value could be ascribed to a time-varying inductance $\dot{L}_P$ whereas in the post-stagnation phase the plasma impedance was probably dominated by enhanced resistance, R_P. For that reason, the neutron emission is supposed to be a multiphase process and we believe that the prolonged neutron emission is connected with the enhanced resistance. We would like to prove this in future experiments.

Recently, we have prepared a deuterium gas-puff in order to interpret experimental results and to compare them with those obtained in other Z-pinch devices. Should we conclude with what we expect from this modification, we do hope that the interpretation of Z-pinch experiments with pure deuterium will be more straightforward in comparison with a heterogeneous mixture of tungsten, carbon, and deuterium ions.

ACKNOWLEDGMENTS

We wish to thank Professor A. S. Kingsep (RRC Kurchatov Institute, Moscow) for his valuable comments and Dr. G. N. Timoshenko (Laboratory of Radiation Biology of JINR, Dubna) for his kind help with Bonner spheres.

This research has been supported by Research Program Nos. LA08024, 1P05ME761, and LC528 of the Ministry of Education and by Grant No. 202-08-P084 of the Grant Agency of the Czech Republic.

APPENDIX: SCATTERED NEUTRONS

The advantage of time-of-flight (TOF) detectors located in mutually opposite directions concerns neutron scattering. A large number of scattered neutrons forms the tail of TOF signals. It causes the shift of measured neutron energies to lower values. So far, the Monte Carlo ray-tracing of neutrons[66] between the neutron source and TOF detectors has been performed only for a small part of the diagnostic arrangement. Therefore, we tested the influence of scattered neutrons on our reconstruction by the use of artificial energy distribution function $f_0(E_n,t)$ which was modified by scattered neutrons (the average energy decrease of about 0.1 MeV). According to this modified distribution function $f_M(E_n,t)$, test neutron signals $S(x,T)$ were generated at the TOF detectors. On the basis of these TOF signals, we wanted to reconstruct the original distribution function $f_0(E,t)$ by our Monte Carlo simulation. In the case of TOF detectors on both sides of the neutron source, it was not possible to simulate a large number of low-energy neutrons in one direction from the neutron source because it required a large number of high-energy neutrons in the opposite direction. As a result, we found out that our Monte Carlo reconstruction suppressed the influence of scattered neutrons and that the test energy spectrum was reconstructed correctly. Including the temporal resolution of TOF detectors, the systematic error of neutron energy reconstruction in our experiment was estimated below 0.1 and 0.05 MeV for the end-on and side-on direction, respectively. With regard to the time of neutron emission, it was a little delayed in comparison with the original test distribution function. Therefore, it seemed more accurate to calculate the emission time from the nearest TOF detector. Of course, due to a small number of TOF detectors, it was not possible to determine unambiguously the shape of the neutron energy spectrum. Yet from the chain of four TOF detectors, two basic moments of the energy distribution function (i.e., the mean energy and the width of spectrum) could be estimated.

[1] T. Sandford, G. Allshouse, B. Marder *et al.*, Phys. Rev. Lett. **77**, 5063 (1996). R. Spielman, C. Deeney, G. Chandler *et al.*, Phys. Plasmas **5**, 2105 (1998).
[2] M. G. Haines, Plasma Phys. Controlled Fusion **38**, 643 (1996); S. W. Cousins and A. A. Ware, Proc. Phys. Soc. London, Sect. B **64**, 159 (1951); P. Thonemann, Nature **181**, 217 (1958).
[3] J. W. Mather and A. H. Williams, in *Proceedings of the 2nd United Nations International Conference on Peaceful Uses of Atomic Energy, Geneva, 1958*, edited by J. H. Martens *et al.* (United Nations, Geneva, Switzerland, 1958), Vol. 32, p. 26; J. L. Tuck, *ibid.*, Vol. 32, p. 3; R. F. Post, Rev. Mod. Phys. **28**, 338 (1956).
[4] O. A. Anderson, W. R. Baker, S. A. Colgate, J. Ise, and R. V. Pyle, Phys. Rev. **110**, 1375 (1958).
[5] A. M. Andrianov, O. A. Bazilevskaia, S. I. Braginski *et al.*, in *Proceedings of the 2nd United Nations International Conference on Peaceful Uses of Atomic Energy, Geneva, 1958*, edited by J. H. Martens *et al.* (United Nations, Geneva, Switzerland, 1958), Vol. 31, p. 348; L. A. Artsimovich, *ibid.*, p. 6; I. V. Kurchatov, At. Energy **1**, 359 (1956).
[6] E. von Funfer, H. Herold, G. Lehner, H. Tuczek, and C. Andelfinger, Z. Naturforsch. A **13A**, 524 (1958); K. Nishiguchi, H. Maruo, Y. Arata, and M. Okada, J. At. Energy Soc. Jpn. **1**, 115 (1959); S. Berglund, R. Nilsson, P. Ohlin, K. Siegbahn, T. Sundstrom, and S. Svennerstedt, Nucl. Instrum. **1**, 233 (1957).
[7] See National Technical Information Service Document No. LA3253 (Review of Controlled Thermonuclear Research at Los Alamos 1965, LANL Rep. LA-3253-MS, 1965). Copies may be ordered from National Technical Information Service, Springfield, VA 22161.
[8] A. Bernard, J. P. Garconnet, A. Jolas, J. P. Le Breton, and J. de Mascureau, in *Plasma Physics and Controlled Fusion Research (IAEA-CN-37), 7th IAEA Conference on Plasma Physics and Controlled Nuclear Fusion, Innsbruck, 1978* (IAEA, Vienna, 1979), Vol. 2, p. 159.
[9] N. V. Filippov, T. I. Filippova, and V. P. Vinogradov, Nucl. Fusion **2**, 577 (1962).
[10] J. E. Hammel, D. W. Scudder, and J. S. Shlachter, Nucl. Instrum. Methods Phys. Res. **207**, 161 (1983).
[11] D. W. Scudder, Bull. Am. Phys. Soc. **30**, 1408 (1985); N. R. Pereira, N. Rostoker, J. Riordan, and M. Gersten, in *Proceedings of the 1st International Conference on Dense Z-Pinches for Fusion, Alexandria, VA, 1984*, edited by J. D. Sethian and K. A. Gerber (Naval Research Laboratory, Washington, DC, 1984), p. 71; J. E. Hammel, D. W. Scudder, and J. S. Schlachter, *ibid.*, p. 13.
[12] J. D. Sethian, A. E. Robson, K. A. Gerber, and A. W. DeSilva, Phys. Rev. Lett. **59**, 892 (1987).
[13] J. Sethian, A. Robson, K. Gerber, and A. DeSilva, *Proceedings of the*

Workshop on Physics of Alternative Magnetic Confinement Schemes, Varenna, 1990, edited by S. Ortolani and E. Sindoni (Editrice Compositori, Bologna, Italy, 1991), p. 511.
[14]D. W. Scudder, *Proceedings on the Workshop on Physics of Alternative Magnetic Confinement Schemes, Varenna, 1990*, edited by S. Ortolani and E. Sindoni (Editrice Compositori, Bologna, Italy, 1991), p. 519.
[15]W. Kies, G. Decker, M. Malzig *et al.*, J. Appl. Phys. **70**, 7261 (1991).
[16]S. V. Lebedev, R. Aliaga-Rossel, J. P. Chittenden, I. H. Mitchell, A. E. Dangor, M. G. Haines, and J. F. Worley, Phys. Plasmas **5**, 3366 (1998).
[17]S. Stephanakis, L. Levine, D. Mosher, I. Vitkovitsky, and F. Young, Phys. Rev. Lett. **29**, 568 (1972); F. Young, S. Stephanakis and D. Mosher, J. Appl. Phys. **48**, 3642 (1977).
[18]K. C. Mittal, K. A. Gerber, and J. D. Sethian, J. Appl. Phys. **70**, 6712 (1991).
[19]S. Lee and H. Conrads, Phys. Lett. **57A**, 233 (1976).
[20]Yu. L. Bakshaev, P. I. Blinov, V. V. Vikhrev *et al.*, Plasma Phys. Rep. **32**, 531 (2006).
[21]V. V. Vikhrev and V. D. Korolev, Plasma Phys. Rep. **33**, 356 (2007).
[22]A. Batyunin, Sov. J. Plasma Phys. **16**, 597 (1990).
[23]A. L. Velikovich, R. W. Clark, J. Davis *et al.*, Phys. Plasmas **14**, 022701 (2007); C. A. Coverdale, C. Deeney, A. L. Velikovich *et al.*, *ibid.* **14**, 022706 (2007); **14**, 056309 (2007).
[24]See National Technical Information Service Document No. DE98007273 (R. B. Spielman *et al.*, D–D fusion experiments using fast Z pinches, Sandia National Laboratories, Rep. SAND98-0705, 1998). Copies may be ordered from National Technical Information Service, Springfield, VA 22161.
[25]I. Mitchell, J. Gomez, S. Lebedev, S. Bland, J. Chittenden, D. Ampleford, S. Bott, and G. Hall, Bull. Am. Phys. Soc. **49**, 334 (2004).
[26]D. Klir, P. Kubes, J. Kravarik *et al.*, Plasma Devices Oper. **13**, 39 (2005).
[27]M. G. Haines, P. D. LePell, C. A. Coverdale, B. Jones, C. Deeney, and J. P. Apruzese, Phys. Rev. Lett. **96**, 075003 (2006).
[28]B. Wolle, Phys. Rep. **312**, 1 (1999).
[29]C. K. Li, F. H. Seguin, D. G. Hicks *et al.*, Phys. Plasmas **8**, 4902 (2001); G. Pretzler, A. Saemann, A. Pukhov *et al.*, Phys. Rev. E **58**, 1165 (1998); T. Ditmire, J. Zweiback, V. P. Yanovky, T. E. Cowan, G. Hays, and K. B. Wharton, Nature **398**, 489 (1999); V. P. Krainov and M. B. Smirnov, Phys. Rep. **370**, 237 (2002).
[30]I. Tiseanu, G. Decker, and W. Kies, Nucl. Instrum. Methods Phys. Res. A **373**, 73 (1996); I. Tiseanu and I. Craciunescu, Nucl. Sci. Eng. **47**, 384 (1996).
[31]K. Rezac, D. Klir, P. Kubes, J. Kravarik, and M. Stransky, Czech. J. Phys. **56**, B357 (2006).
[32]K. Rezac, D. Klir, J. Kravarik *et al.*, *Conference Proceedings of Contributed Papers, 34th EPS Conference on Plasma Physics, Warsaw, 2007*, edited by P. Gasior and J. Wolowski (European Physical Society, Petit Lancy, 2007), Vol. 31F, p. P-1.016.
[33]M. Drosg and O. Schwerer, in *Production of Monoenergetic Neutrons Between 0.01 and 23 MeV*, Handbook of Nuclear Activation Data (IAEA, Vienna, 1987), p. 111.
[34]M. B. Chadwick, P. Oblozinsky, M. Herman *et al.*, Nucl. Data Sheets **107**, 2931 (2006).
[35]A. S. Chernenko, Yu. M. Gorbulin, Yu. G. Kalinin *et al.*, in *Proceedings of the 11th International Conference on High Power Particle Beams, Prague, 1996*, edited by J. Ullschmied (Academy of Science of Czech Republic, Prague, 1996), Vol. 1, p. 154; Yu. L. Bakshaev, A. S. Chernenko, V. D. Korolev *et al.*, *ibid.*, Vol. 2, p. 962.
[36]Yu. L. Bakshaev, P. I. Blinov, A. S. Chernenko *et al.*, Rev. Sci. Instrum. **72**, 1210 (2001).
[37]D. Klir, P. Kubes, and J. Kravarik, IEEE Trans. Plasma Sci. **34**, 2303 (2006).
[38]A. Velyhan, J. Krasa, B. Bienkowska *et al.* Phys. Scr., T **123**, 112 (2006).
[39]D. D. Ryutov, M. S. Derzon, and M. K. Matzen, Rev. Mod. Phys. **72**, 167 (2000).
[40]M. G. Haines, Laser Part. Beams **19**, 345 (2001).
[41]L. Soto, Plasma Phys. Controlled Fusion **47**, A361 (2005); Y. Mizuguchi, J. I. Sakai, H. R. Yousefi, T. Haruki, and K. Masugata, Phys. Plasmas **14**, 032704 (2007); V. A. Gribkov, A. Banaszak, B. Bienkowska *et al.*, J. Phys. D **40**, 3592 (2007).
[42]M. J. Bernstein and G. G. Comisar, Phys. Fluids **15**, 700 (1972).
[43]A. Bernard, A. Coudeville, A. Jolas, J. Lauspach, and J. de Mascreau, Phys. Fluids **18**, 180 (1975).
[44]I. H. Mitchell, R. Aliaqa-Rossel, J. P. Chittenden, A. Robledo, H. Schmidt, and M. G. Haines, IEEE Trans. Plasma Sci. **26**, 1267 (1998).
[45]H. Schmidt, P. Kubes, M. Sadowski, and M. Scholz, IEEE Trans. Plasma Sci. **34**, 2363 (2006).
[46]G. Belyaev, M. Basko, A. Cherkasov *et al.*, Phys. Rev. E **53**, 2701 (1996).
[47]J. F. Ziegler, Nucl. Instrum. Methods Phys. Res. B **219-220**, 1027 (2004).
[48]H. A. Bodin, R. A. Fitch, and N. J. Peacock, J. Nucl. Energy, Part C **1**, 206 (1960).
[49]M. G. Haines, Nucl. Instrum. Methods Phys. Res. **207**, 179 (1983); G. McCall, Phys. Rev. Lett. **62**, 1986 (1989).
[50]M. J. Bernstein, Phys. Rev. Lett. **24**, 724 (1970); M. J. Bernstein and F. Hai, *ibid.* **25**, 641 (1970).
[51]T. Yamamoto, K. Shimoda, K. Kobayashi, and K. Hirano, Jpn. J. Appl. Phys., Part 1 **23**, 242 (1984).
[52]W. Kies, G. Decker, U. Berntien, Yu. V. Sidelnikov, D. A. Gluskov, K. N. Koshelev, D. M. Simanovskii, and S. V. Bobashev, Plasma Sources Sci. Technol. **9**, 279 (2000).
[53]P. Kubes, J. Kravarik, D. Klir *et al.*, IEEE Trans. Plasma Sci. **34**, 2349 (2006).
[54]B. A. Trubnikov, Sov. J. Plasma Phys. **12**, 271 (1986).
[55]H. S. Uhm and T. N. Lee, Phys. Rev. A **40**, 3915 (1989).
[56]G. Decker, W. Kies, and G. Pross, Phys. Fluids **26**, 571 (1983).
[57]A. Bernard, Atomkernenergie **32**, 73 (1978).
[58]R. B. Spielman, J. S. DeGroot, T. J. Nash, J. McGurn, L. Ruggles, M. Vargas, and K. G. Estabrook, AIP Conf. Proc. **299**, 404 (1994).
[59]L. I. Rudakov, A. L. Velikhovich, J. Davis, J. W. Thornhill, J. L. Giuliani, and C. Deeney, Phys. Rev. Lett. **84**, 3326 (2000).
[60]J. Riordan, J. Pearlman, M. Gersten, and J. Rauch, AIP Conf. Proc. **75**, 35 (1981).
[61]K. G. Whitney, J. W. Thornhill, J. P. Apruzese, J. Davis, C. Deeney, and C. A. Coverdale, Phys. Plasmas **11**, 3700 (2004).
[62]J. P. Chittenden, S. V. Lebedev, C. A. Jennings, S. N. Bland, and A. Ciardi, Plasma Phys. Controlled Fusion **46**, B457 (2004).
[63]V. V. Vikhrev, Sov. J. Plasma Phys. **12**, 262 (1986).
[64]V. V. Vikhrev, Sov. J. Plasma Phys. **15**, 339 (1989).
[65]R. Riley, D. Scudder, J. Shlachter, and R. Lovberg, Phys. Plasmas **3**, 1314 (1996).
[66]See National Technical Information Service Document No. DE87000708 (J. F. Briesmeister, MCNP: A general Monte Carlo code for neutron and photon transport, LANL Report, 1986). Copies may be ordered from National Technical Information Service, Springfield, VA 22161.